

Tailoring of Fe/MnK-CNTs Composite Catalysts for the Fischer–Tropsch Synthesis of Lower Olefins from Syngas

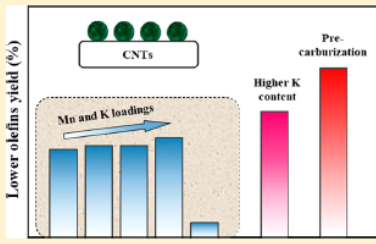
Bingxu Chen,^{†,‡} Xinxin Zhang,[†] Wenyao Chen,[†] Di Wang,[†] Nan Song,[†] Gang Qian,[†] Xuezhi Duan,^{*,†,⊙} Jia Yang,[‡] De Chen,[‡] Weikang Yuan,[†] and Xinggui Zhou[†]

[†]State Key Laboratory of Chemical Engineering, East China University of Science and Technology, 130 Meilong Road, Shanghai 200237, China

[‡]Department of Chemical Engineering, Norwegian University of Science and Technology, Trondheim 7491, Norway

Supporting Information

ABSTRACT: Iron-catalyzed conversion of coal/biomass-derived syngas directly to lower olefins through Fischer–Tropsch synthesis (i.e., FTO) is a sustainable and short-flow process. Herein, effects of Mn and K promoter loadings on FTO performance over the Fe-based catalyst supported on the promoter-adjustable carbon nanotubes (Fe/Mn_xK_y-CNTs) are systematically studied. Several Mn_xK_y-CNTs are prepared by the treatment of CNTs using aqueous KMnO₄ solution via a redox reaction, where promoter loadings are tailored by changing the aqueous KMnO₄ solution concentration and water amount for sample washing. FTO performance of these catalysts suggests that the increase in Mn and K loadings shows the enhanced lower olefins selectivity but suppressed activity. The resultant Fe/Mn_{16.5}K_{1.2}-CNTs exhibit the highest lower olefins yield. Further increasing K promoter content leads to slightly enhanced activity to lower olefins but dramatically suppressed CH₄ formation and enhanced chain growth. Moreover, appropriate pre-carburization temperature can facilitate the activity and selectivity toward lower olefins formation.



1. INTRODUCTION

The direct conversion of coal/biomass-derived syngas with low H₂/CO ratio to lower olefins (C₂–C₄) without additional intermediate steps, i.e., Fischer–Tropsch-to-olefins (FTO), is of burgeoning scientific and industrial interest.^{1–6} Over the past decades, a variety of catalysts, e.g., Co, Ru and Fe, were commonly employed for the Fischer–Tropsch synthesis.^{7–11} Among them, the low-cost Fe-based catalyst is suggested as the most attractive one for several reasons, such as its high selectivity to C₂–C₄ and its ability to directly convert CO-rich syngas without preadjustment of H₂/CO ratio.^{12–20} Compared to the bulk iron catalysts, the supported ones are more appropriate for the industry applications under harsh reaction conditions, because the stability of the supported catalysts is mechanically higher and the active phase dispersion on them is better.^{12–17} There is a consensus that when the α -Al₂O₃ and carbon material are used to support the iron the resultant Fe-based catalysts especially in the presence of promoters can produce high yield of lower olefins due to the weak metal–support interaction.^{1,12–17}

Manganese and potassium are two widely used promoters in the iron-based FTO process to promote the formation of lower olefins.^{16,21–28} Typically, the addition of manganese usually suppresses methane formation and secondary hydrogenation of lower olefins, resulting in a high lower olefins selectivity. However, during the heat treatment, manganese species tend to form mixed oxides with iron species due to their similar

ionic radii,^{22,23} which are unfavorable for the subsequent reduction and essential carburization. On the other hand, the promotional effect of K for the Fe-based catalysts is a hot topic for the FTO process.^{16,24–29} Appropriate potassium loading can facilitate iron carburization, and thus enhance the catalytic activity and improve the long chain hydrocarbons (C₅₊) formation. Therefore, simultaneously adding Mn and K to the Fe catalysts is a promising strategy to obtain high yield of lower olefins.

Recently, a kind of highly dispersed K-doped MnO₂ coated Fe-based catalyst, named as Fe/MnK-CNTs, has been prepared by a novel method.^{30,31} In this method, the resultant K- and Mn-coated carbon nanotubes, named as MnK-CNTs, from the treatment of CNTs using aqueous KMnO₄ solution via a redox reaction, were used to immobilize the iron precursor followed by thermal treatments. This novel nanocomposite has a good FTO performance due to its well-distributed promoters, uniform iron nanoparticles, more defects on the CNTs, and weak metal–support interactions. Furthermore, the optimized calcination temperature was identified as 220 °C to gain the highest selectivity to lower olefins as well as good stability among several of these

Received: April 25, 2018

Revised: August 3, 2018

Accepted: August 9, 2018

Published: August 9, 2018

nanocomposites through different calcination temperatures.³¹ The amounts of potassium and manganese of these nanocomposites remain the same. It is worth mentioning that the promoters content could affect the Fischer–Tropsch synthesis performance dramatically.^{15,16,32,33} Herein, as a consecutive effort, manganese and potassium promoter loadings, easily adjusted by changing the preparation conditions, will be tailored toward optimizing the FTO performance.

Herein, several Fe/Mn_xK_y-CNTs catalysts consisting of different Mn and K loadings were first synthesized by changing the preparation conditions of Mn_xK_y-CNTs support. Then, all of these Fe/Mn_xK_y-CNTs catalysts were tested for the FTO performance. Also, they were characterized by several techniques, such as XRD, Raman, H₂-TPR, and TEM. The optimized Fe/Mn_{16.5}K_{1.2}-CNTs catalyst was identified with the highest lower olefins yield. Furthermore, the introduction of more potassium promoter and the role of the precarburization under different temperatures were investigated. These results demonstrated the importance of modulating the promoters content of the novel Fe/Mn_xK_y-CNTs composites, which is helpful to fabricate the promoted iron-based FTO catalysts toward high FTO performance.

2. EXPERIMENTAL SECTION

2.1. Catalyst Preparation. Pristine CNTs with closed ends were modified in HNO₃ to increase the hydrophilicity of the carbon surface. At first, the pristine CNTs were dispersed into HNO₃ and refluxed at 120 °C for 2 h. After that, the samples in the HNO₃ solutions were filtered to remove the acid, and the deionized water was further added to remove the residual acid for several times to neutral pH. The samples were further dried in an oven at 120 °C for a whole night. Potassium-doped MnO₂ coated carbon nanotubes were prepared by the treatment of CNTs using aqueous KMnO₄ solution via a redox reaction according to our previous method.^{30,31} Typically, the modified CNTs were treated by different concentrated aqueous KMnO₄ solutions (i.e., 0.01–0.1 M) to form a uniform mixture under magnetic stirring. During the reaction, the temperature was kept at 70 °C by a water bath. After the treatment of the CNTs, the products with the aqueous reaction solution were filtered and washed with different amounts of deionized water (i.e., 1–3 L). The as-obtained Mn_xK_y-CNTs were further desiccated for the whole night in stagnant air under 120 °C, where the loadings of Mn and K were measured by ICP-AES.

The Fe/Mn_xK_y-CNTs catalysts were further prepared by incipient wetness impregnation method. Typically, the Mn_xK_y-CNTs were mixed with Fe precursor (ferric nitrate), and the loading of iron was kept as 10 wt %. The obtained catalysts were aged under static air and 25 °C for 24 h. The aged catalysts were then desiccated at 120 °C for 12 h. After that, the samples were calcined under a nitrogen flow at the optimized calcination temperature for the Fe/Mn_xK_y-CNTs FTO catalysts, i.e., 220 °C, for 3 h according to our previous work.³¹

2.2. Catalyst Characterization. Inductively coupled plasma-atomic emission spectroscopy (ICP-AES) for the precise measurement of the metal loadings of Mn and K over the Mn_xK_y-CNTs were performed on the Agilent 725ES instrument made in the U.S.A. X-ray diffraction (XRD) for the determination of the crystal phases over the samples was carried out on a Rigaku D/Max2550VB/PC X-ray diffractometer instrument from Japan with Cu K α radiation ($\lambda =$

1.54056 Å). Transmission electron microscopy (TEM) for the measurement of the microstructures over the samples was performed on the JEM-2100 instrument made from JEOL in Japan. Raman spectroscopy to characterize surface chemistry properties of the samples was performed and recorded at room temperature on a microscope (inVia Reflex, Renishaw, U.K.) using a 2 mW laser power at 514 nm laser excitation according to the previous studies.³⁴ H₂ temperature-programmed reduction (H₂-TPR) for the evaluation of the reducibility of the calcined samples was performed over an Autochem 2920 instrument made from Micromeritics in the U.S.A. For the H₂-TPR, the corresponding H₂ intensity were quantified by a thermal conductivity detector (TCD). The temperature was increased from 25 to 800 °C, and the heating rate is 10 °C every minute. Thermal gravimetric-differential thermal analysis (TGA-DTA) of the carburized samples was conducted on a TA SDT-Q600 thermobalance under an air flow from 30 to 800 °C with the heating rate of 10 °C every minute. It is worth noting that, before the characterizations, the Mn_xK_y-CNTs and the Fe/Mn_xK_y-CNTs samples were first reduced under H₂ flow at 300 °C for 10 h in the reactor. Before the catalysts were taken from the reactor, they were passivated in 0.92% O₂/Ar at room temperature.

2.3. Catalytic Testing. The performance of the Mn_xK_y-CNTs supported Fe catalysts for FTO was tested by a fixed-bed reactor made of stainless steel. In a typical experiment, 100 mg of catalyst was placed in the reactor. Before the reaction, the temperature was raised to 300 °C under N₂ flow. Then, the hydrogen was introduced to reduce the catalyst for 10 h at 300 °C and ambient pressure. When the reduction process was finished, the reactor was cooled to 270 °C under N₂ atmosphere. After the reduction, the feed gas was switched to syngas (H₂/CO = 1). The corresponding GHSV was set as 30 000 mL h⁻¹ g_{cat}⁻¹. Simultaneously, the system pressure was adjusted to 2 MPa. The analyses of the outlet products were performed in a gas chromatograph made in Echrom from China. The detailed analysis method as well as the activity and selectivity calculations are performed according to our previously reported literatures.^{30,31}

3. RESULTS AND DISCUSSION

3.1. Characterization. Mn and K well dispersed carbon nanotubes, named as Mn_xK_y-CNTs, were prepared by the treatment of CNTs using aqueous KMnO₄ solution via a redox reaction, i.e., 4MnO₄⁻ + 3C + H₂O → 4MnO₂ + CO₃²⁻ + 2HCO₃⁻, generating a MnO₂ coating layer with a strong interaction with carbon support surface.^{35,36} The loadings of Mn and K were tailored by changing the concentration of aqueous KMnO₄ solution and the amount of water for sample washing, respectively. The resultant CNTs were labeled as Mn_xK_y-CNTs, in which *x* and *y* correspond to Mn and K loadings, respectively. Table 1 shows five kinds of Mn_xK_y-CNTs with different Mn and K loadings determined by ICP-AES. Clearly, there are significantly different Mn loadings but slightly different K loadings.

The five as-prepared Mn_xK_y-CNTs were used as supports to further immobilize the Fe by incipient wetness impregnation method. The corresponding Fe loadings were kept as 10 wt % for all of the Fe/Mn_xK_y-CNTs catalysts. The iron-catalyzed FTO performance has been found to have dependence on the Fe particle size and morphology.^{14,37} Herein, we employed TEM to characterize the microstructures of the five catalysts. The representative TEM images of the samples were illustrated

nanocomposites through different calcination temperatures.³¹ The amounts of potassium and manganese of these nanocomposites remain the same. It is worth mentioning that the promoters content could affect the Fischer–Tropsch synthesis performance dramatically.^{15,16,32,33} Herein, as a consecutive effort, manganese and potassium promoter loadings, easily adjusted by changing the preparation conditions, will be tailored toward optimizing the FTO performance.

Herein, several Fe/Mn_xK_y-CNTs catalysts consisting of different Mn and K loadings were first synthesized by changing the preparation conditions of Mn_xK_y-CNTs support. Then, all of these Fe/Mn_xK_y-CNTs catalysts were tested for the FTO performance. Also, they were characterized by several techniques, such as XRD, Raman, H₂-TPR, and TEM. The optimized Fe/Mn_{1.65}K_{1.2}-CNTs catalyst was identified with the highest lower olefins yield. Furthermore, the introduction of more potassium promoter and the role of the precarburization under different temperatures were investigated. These results demonstrated the importance of modulating the promoters content of the novel Fe/Mn_xK_y-CNTs composites, which is helpful to fabricate the promoted iron-based FTO catalysts toward high FTO performance.

2. EXPERIMENTAL SECTION

2.1. Catalyst Preparation. Pristine CNTs with closed ends were modified in HNO₃ to increase the hydrophilicity of the carbon surface. At first, the pristine CNTs were dispersed into HNO₃ and refluxed at 120 °C for 2 h. After that, the samples in the HNO₃ solutions were filtered to remove the acid, and the deionized water was further added to remove the residual acid for several times to neutral pH. The samples were further dried in an oven at 120 °C for a whole night. Potassium-doped MnO₂ coated carbon nanotubes were prepared by the treatment of CNTs using aqueous KMnO₄ solution via a redox reaction according to our previous method.^{30,31} Typically, the modified CNTs were treated by different concentrated aqueous KMnO₄ solutions (i.e., 0.01–0.1 M) to form a uniform mixture under magnetic stirring. During the reaction, the temperature was kept at 70 °C by a water bath. After the treatment of the CNTs, the products with the aqueous reaction solution were filtered and washed with different amounts of deionized water (i.e., 1–3 L). The as-obtained Mn_xK_y-CNTs were further desiccated for the whole night in stagnant air under 120 °C, where the loadings of Mn and K were measured by ICP-AES.

The Fe/Mn_xK_y-CNTs catalysts were further prepared by incipient wetness impregnation method. Typically, the Mn_xK_y-CNTs were mixed with Fe precursor (ferric nitrate), and the loading of iron was kept as 10 wt %. The obtained catalysts were aged under static air and 25 °C for 24 h. The aged catalysts were then desiccated at 120 °C for 12 h. After that, the samples were calcined under a nitrogen flow at the optimized calcination temperature for the Fe/Mn_xK_y-CNTs FTO catalysts, i.e., 220 °C, for 3 h according to our previous work.³¹

2.2. Catalyst Characterization. Inductively coupled plasma-atomic emission spectroscopy (ICP-AES) for the precise measurement of the metal loadings of Mn and K over the Mn_xK_y-CNTs were performed on the Agilent 725ES instrument made in the U.S.A. X-ray diffraction (XRD) for the determination of the crystal phases over the samples was carried out on a Rigaku D/Max2550VB/PC X-ray diffractometer instrument from Japan with Cu K α radiation (λ =

1.54056 Å). Transmission electron microscopy (TEM) for the measurement of the microstructures over the samples was performed on the JEM-2100 instrument made from JEOL in Japan. Raman spectroscopy to characterize surface chemistry properties of the samples was performed and recorded at room temperature on a microscope (inVia Reflex, Renishaw, U.K.) using a 2 mW laser power at 514 nm laser excitation according to the previous studies.³⁴ H₂ temperature-programmed reduction (H₂-TPR) for the evaluation of the reducibility of the calcined samples was performed over an Autochem 2920 instrument made from Micromeritics in the U.S.A. For the H₂-TPR, the corresponding H₂ intensity were quantified by a thermal conductivity detector (TCD). The temperature was increased from 25 to 800 °C, and the heating rate is 10 °C every minute. Thermal gravimetric-differential thermal analysis (TGA-DTA) of the carburized samples was conducted on a TA SDT-Q600 thermobalance under an air flow from 30 to 800 °C with the heating rate of 10 °C every minute. It is worth noting that, before the characterizations, the Mn_xK_y-CNTs and the Fe/Mn_xK_y-CNTs samples were first reduced under H₂ flow at 300 °C for 10 h in the reactor. Before the catalysts were taken from the reactor, they were passivated in 0.92% O₂/Ar at room temperature.

2.3. Catalytic Testing. The performance of the Mn_xK_y-CNTs supported Fe catalysts for FTO was tested by a fixed-bed reactor made of stainless steel. In a typical experiment, 100 mg of catalyst was placed in the reactor. Before the reaction, the temperature was raised to 300 °C under N₂ flow. Then, the hydrogen was introduced to reduce the catalyst for 10 h at 300 °C and ambient pressure. When the reduction process was finished, the reactor was cooled to 270 °C under N₂ atmosphere. After the reduction, the feed gas was switched to syngas (H₂/CO = 1). The corresponding GHSV was set as 30 000 mL h⁻¹ g_{cat}⁻¹. Simultaneously, the system pressure was adjusted to 2 MPa. The analyses of the outlet products were performed in a gas chromatograph made in Echrom from China. The detailed analysis method as well as the activity and selectivity calculations are performed according to our previously reported literatures.^{30,31}

3. RESULTS AND DISCUSSION

3.1. Characterization. Mn and K well dispersed carbon nanotubes, named as Mn_xK_y-CNTs, were prepared by the treatment of CNTs using aqueous KMnO₄ solution via a redox reaction, i.e., $4\text{MnO}_4^- + 3\text{C} + \text{H}_2\text{O} \rightarrow 4\text{MnO}_2 + \text{CO}_3^{2-} + 2\text{HCO}_3^-$, generating a MnO₂ coating layer with a strong interaction with carbon support surface.^{35,36} The loadings of Mn and K were tailored by changing the concentration of aqueous KMnO₄ solution and the amount of water for sample washing, respectively. The resultant CNTs were labeled as Mn_xK_y-CNTs, in which *x* and *y* correspond to Mn and K loadings, respectively. Table 1 shows five kinds of Mn_xK_y-CNTs with different Mn and K loadings determined by ICP-AES. Clearly, there are significantly different Mn loadings but slightly different K loadings.

The five as-prepared Mn_xK_y-CNTs were used as supports to further immobilize the Fe by incipient wetness impregnation method. The corresponding Fe loadings were kept as 10 wt % for all of the Fe/Mn_xK_y-CNTs catalysts. The iron-catalyzed FTO performance has been found to have dependence on the Fe particle size and morphology.^{14,37} Herein, we employed TEM to characterize the microstructures of the five catalysts. The representative TEM images of the samples were illustrated

Table 1. Mn and K Loadings of Five Kinds of Mn_xK_y -CNTs Samples

samples	Mn (wt %)	K (wt %)
$Mn_{5.3}K_{0.9}$ -CNTs	5.3	0.9
$Mn_{8.3}K_{1.0}$ -CNTs	8.3	1.0
$Mn_{12.4}K_{1.1}$ -CNTs	12.4	1.1
$Mn_{16.5}K_{1.2}$ -CNTs	16.5	1.2
$Mn_{23.0}K_{1.3}$ -CNTs	23.0	1.3

in Figure 1. Obviously, no big aggregates appear over all of the catalysts, possibly because the existence of manganese can inhibit the aggregation of the iron nanoparticles.³⁸ Their average particle sizes are 8.5 ± 2.7 , 9.9 ± 2.7 , 9.9 ± 1.6 , 9.8 ± 2.2 , and 9.6 ± 2.4 nm, respectively. This indicates that the average Fe particle size is not highly dependent on the Mn and K loadings of Mn_xK_y -CNTs.

The XRD was performed for the five calcined Fe/Mn_xK_y -CNTs catalysts and the corresponding reduced ones to explore their crystal phase and catalyst compositions. The obtained XRD patterns for the reduced and calcined samples are shown in Figure 2a and Figure S1, respectively. For the calcined samples, the carbon nanotubes show clear characteristic diffraction peaks (JCPDS No. 65-6212) as well as ones above 30° , very possibly attributed to the mixed metal oxides phases.^{30,31} For the reduced samples, however, there are legible characteristic diffraction peaks for iron manganese oxide ($FeMn_2O_4$, JCPDS No. 75-0035) in addition to ones of carbon support, manganosite (MnO , JCPDS No. 07-0230) and wustite (FeO , JCPDS No. 46-1312). Figure 2b shows a representative HRTEM image, in which the corresponding FFT, i.e., fast Fourier transform, of the selected area were included. Obviously, the 0.256 nm-long lattice spacing was found, which is in good accordance with that of the (311)

plane of spinel $FeMn_2O_4$. Therefore, both the XRD and HRTEM results suggest the formation of the $FeMn_2O_4$ phase.

H_2 -TPR was employed to investigate the reducibility of metal species over the Fe/Mn_xK_y -CNTs catalyst and Mn_xK_y -CNTs samples, and the results are shown in Figure 3. For the Mn_xK_y -CNTs samples, the H_2 -TPR profiles mainly show two reduction peaks lower than $500^\circ C$. The first peak is assigned to the transformation of MnO_2 to Mn_2O_3 , while the second peak to the reduction of Mn_2O_3 to MnO .^{30,31} Meanwhile, there exists a decreased trend for the reduction temperatures with the increase in the Mn and K loadings to 16.5 and 1.2 wt %, followed by an increased trend with a further increase in the Mn and K loadings to 23.0 and 1.3 wt %. This is most likely ascribed to the fact that the manganese oxide coating layer interacts strongly to the carbon support surface and the coating layer is too thick, respectively. Moreover, for the Fe/Mn_xK_y -CNTs catalysts, when the Mn and K loadings were further increased, the corresponding reduction peaks move toward higher temperature, which could be due to that the iron species are strongly interacted with coating layer and/or support.

The different surface chemistry of carbon supports over iron catalysts may result in different FTO performance.³⁹ Generally, the heat treatment (e.g., calcination and reduction) could remove several functional groups over the carbon surface and introduce some surface defects on carbon, which have been proved to show different catalytic performance for the supported metal nanoparticles.^{39,40} Moreover, the introduction of Mn and K would also change the surface chemistry of carbon support, because they could form some coating layers on the carbon surface. Herein, Raman is employed to characterize the surface chemistry of these five catalysts. As shown in Figure 4, the Raman spectra are deconvoluted by using the D_3 peak treated with Gaussian-shaped band and the other four peaks, i.e., D_1 , D_2 , D_4 , and G, treated with Lorentzian-shaped bands.⁴¹ The I_{D1}/I_G value increases with the

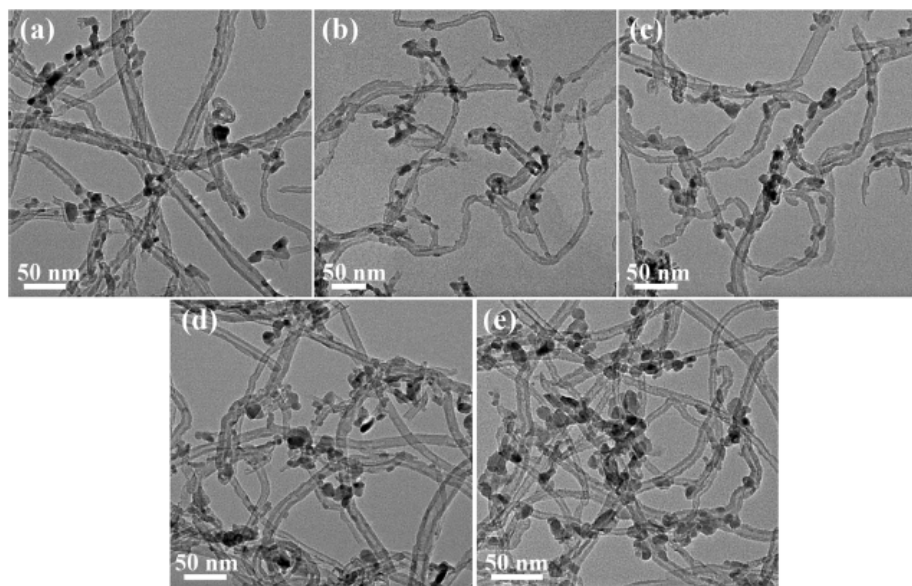


Figure 1. TEM images of the five Fe/Mn_xK_y -CNTs composites after reduction: (a) $Fe/Mn_{5.3}K_{0.9}$ -CNTs, (b) $Fe/Mn_{8.3}K_{1.0}$ -CNTs, (c) $Fe/Mn_{12.4}K_{1.1}$ -CNTs, (d) $Fe/Mn_{16.5}K_{1.2}$ -CNTs, and (e) $Fe/Mn_{23.0}K_{1.3}$ -CNTs.

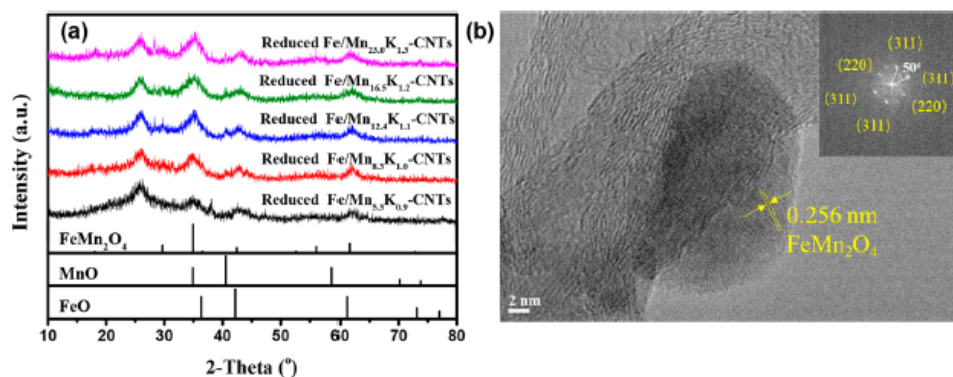


Figure 2. (a) XRD patterns of the Fe/Mn_xK_y-CNTs composites after reduction. The lower part also shows the standard patterns of wustite (JCPDS No. 46-1312), manganosite (JCPDS No. 07-0230) and iron manganese oxide (JCPDS No. 75-0035) for comparison. (b) Representative HRTEM image with its corresponding FFT pattern of the Fe/Mn_{16.5}K_{1.2}-CNTs catalyst.

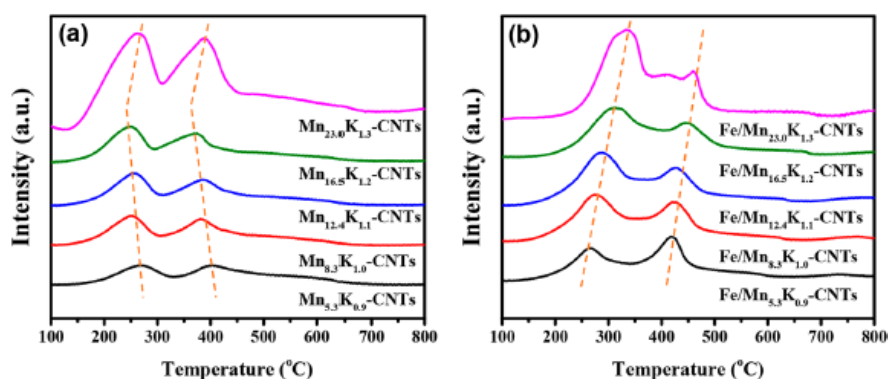


Figure 3. H₂-TPR profiles of (a) Mn_xK_y-CNTs and (b) calcined Fe/Mn_xK_y-CNTs catalysts.

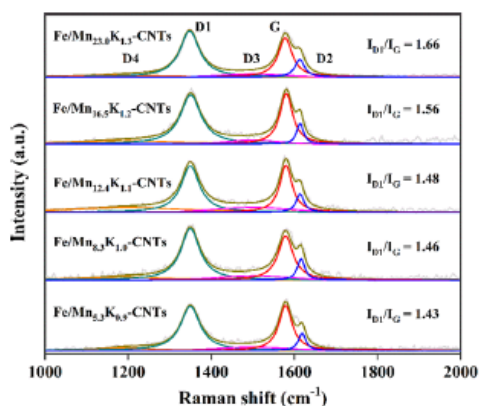


Figure 4. Raman spectra of the Fe/Mn_xK_y-CNTs catalysts after reduction.

Mn and K loadings of the catalysts, indicating more surface defects on the CNTs support arising from the stronger oxidation of CNTs by higher KMnO₄ concentration.

3.2. FTO Performance. Catalytic testing of the five catalysts without precarburization was performed in a fixed-bed reactor. The detailed calculated FTO performance is summarized in Table S1. Obviously, the FTY values, representing the catalytic activity, gradually decrease with the increase of Mn and K loadings, while the catalysts have no

significant difference in the average metal particle sizes (Figure 1). Previous studies showed that the increase in the K loading is favorable for the iron carburization, while that in the Mn loading is unfavorable for the iron carburization. Moreover, there are increased iron reduction temperatures (Figure 3b) and surface defects on the carbon support (Figure 4), which are unfavorable and favorable for the iron carburization, respectively. Thus, we can deduce that the declined activity mainly arises from the increased Mn content and iron reduction temperature, which can inhibit the iron carburization.

Furthermore, the lower olefins selectivity is another important issue beside the activity. Figure 5 illustrates that with the increase of Mn and K loadings, the catalysts show enhanced lower olefin selectivity and suppressed CH₄ and C₅₊ selectivities. In previous work, introduction of K promoter has been reported to mainly adjust the products toward long-chain hydrocarbons and thus boost C₅₊ selectivity, while the Mn promoter to increase the C₂=-C₄= selectivity and to suppress CH₄ formation. Herein, based on the above results, the Mn loading is suggested as a dominant factor for the product selectivity over the five Fe/Mn_xK_y-CNTs composite catalysts. Notably, considering that increasing the Mn loading of the catalysts can simultaneously decrease the activity and increase the selectivity to lower olefins, the Fe/Mn_{16.5}K_{1.2}-CNTs catalyst gives rise to the highest lower olefins yield (Figure 5).

Furthermore, based on the optimized Fe/Mn_{16.5}K_{1.2}-CNTs catalyst mentioned above, effects of K promoter content on the

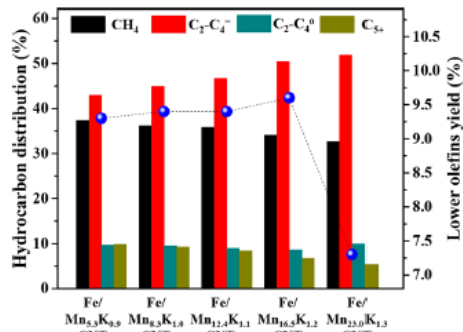


Figure 5. Product distribution and lower olefins yield (blue cycles) of Fe/Mn_xK_y-CNTs catalysts.

FTO performance were studied. The detailed calculated FTO performance results are shown in Table 2. Obviously, higher K

Table 2. FTO Performances of Fe/Mn_xK_y-CNTs Samples with Different K Loadings

catalysts	Fe/Mn _{16.5} K _{1.2} -CNTs	Fe/Mn _{17.0} K _{3.0} -CNTs
CO conversion (%)	28.9	30.1
CH selectivity (%C)	65.5	66.0
FTY ($\mu\text{mol}_{\text{CO}} \text{g}_{\text{Fe}}^{-1} \text{s}^{-1}$)	322.6	338.6
CH distribution (%C)		
CH ₄	34.1	17.2
C ₂ ⁻ -C ₄ ⁻	50.5	51.7
C ₂ ⁰ -C ₄ ⁰	8.6	9.0
C ₅₊	6.8	22.1
olefin/paraffin ratio	5.9	5.7

^aThe detailed testing conditions are same as those shown in Table S1, which are listed in section 2.

content gives rise to slightly enhanced activity to lower olefins, while the remarkably suppressed CH₄ formation as well as the enhanced C₅₊ selectivity, indicating addition of K promoters to the Fe/Mn_xK_y-CNTs catalysts may significantly influence the FTO performance.

3.3. Effects of Carburization Temperature. Precarburization of the optimized Fe/Mn_{16.5}K_{1.2}-CNTs catalyst mentioned above was performed by using the syngas under ambient pressure and different temperatures varying from 210 to 300 °C. After the carburization, the reaction temperature

and pressure were adjusted to 270 °C and 2 MPa for the reaction, respectively. Figure 6a shows the relationship between CO conversion and time on stream for precarburized samples under various temperature. It is found that the higher precarburization temperature leads to the lower CO conversion. This could be most likely because the higher precarburization temperature could cause the formation of larger iron nanoparticles and more carbon deposits on the iron surface based on previous studies.^{17,42}

Moreover, as shown in Table S2, the higher precarburization temperature leads to the increase in the CH₄ selectivity as well as the decrease in the C₅₊ selectivity. On the other hand, the selectivity to lower olefins slightly increases with the precarburization temperature to maximum, i.e., 52.7%, at the precarburization temperature of 230 °C, while the further increased precarburization temperature leads to a decline for the C₂⁻-C₄⁻ selectivity. Previously, it has been reported by De Jong's group that the larger particle size of the active phase of the Fe-based catalyst would result in a decrease in the selectivity to CH₄.¹⁴ On the other hand, although the carbon deposits usually cause the decreased activity, they also give rise to the high coverage of hydrogen and thus relatively high selectivity to CH₄.^{12,43} Herein, we can conclude that the carbon deposits instead of the larger iron nanoparticles formation as the dominant factor leading to product selectivities.

In order to reveal the difference in the carbon deposits for the samples obtained by different precarburization temperature, TGA analyses were carried out for the catalysts after precarburization under low (210 °C) and high (300 °C) temperature. Figure 7 illustrates the detailed TGA-DTG curves. Obviously, there is no obvious mass change but the delayed peak in the DTG curve when the catalyst was carburized under high temperature. This may be because some graphitic coke deposits are formed on the catalyst under high temperature.^{44,45}

Based on the above analyses, compared to the catalyst without precarburization (Figure 5), the precarburization at low temperature (<270 °C) gives rise to the increased lower olefins yield (Figure 6b), indicating that suitable precarburization temperature could enhance the FTO performance of the Fe/Mn_xK_y-CNTs composite catalyst. Moreover, when the precarburization temperature is 230 °C, the catalyst exhibits the highest lower olefins yield of 11.4%.

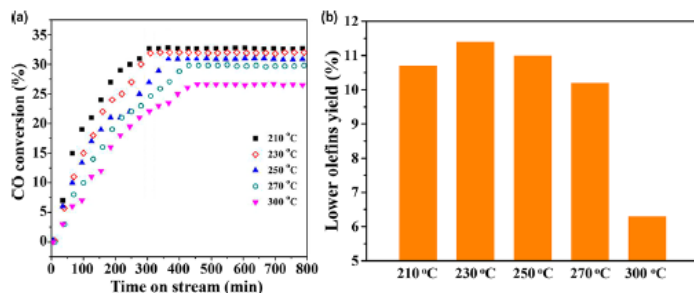


Figure 6. Relationship between CO conversion and TOS (a) and the C₂⁻-C₄⁻ yield (b) of Fe/Mn_{16.5}K_{1.2} samples precarburized under different temperatures.

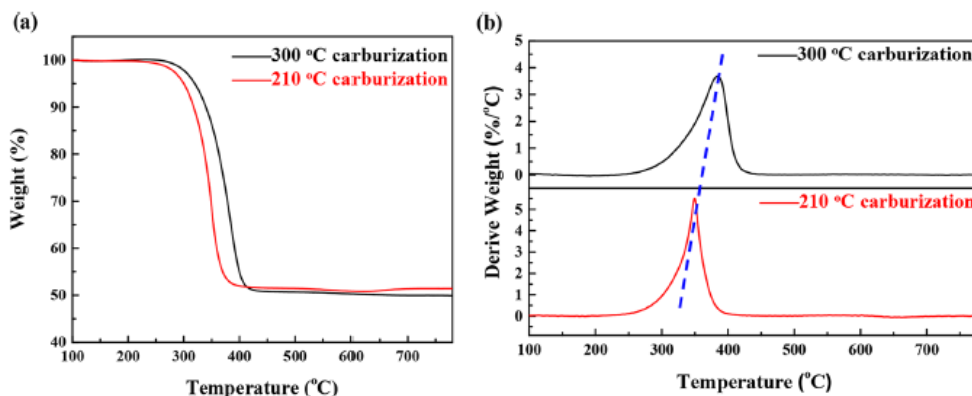


Figure 7. (a) TGA and (b) DTG curves of the Fe/Mn_{16.5}K_{1.2} catalysts after carburization under 210 (red line) and 300 °C (black line).

4. CONCLUSIONS

In summary, Fe/Mn_xK_y-CNTs composite catalysts with different Mn and K loadings have been manipulated through a novel method, i.e., treating CNTs using aqueous KMnO₄ solution via a redox reaction, for the FTO. The promoter loadings are successfully tailored by changing the aqueous KMnO₄ solution concentration and water amount for sample washing. Increasing the Mn and K loadings shows the promoted C₂=-C₄= selectivity but the suppressed activity, and the resultant Fe/Mn_{16.5}K_{1.2}-CNTs exhibits the highest yield of lower olefins. Based on such optimized catalyst, a further increase in the K promoter content only gives rise to slightly enhanced activity to lower olefins but the dramatically suppressed CH₄ formation and enhanced chain growth. Moreover, appropriate precarburization temperature can facilitate the activity and selectivity toward C₂=-C₄= formation. These insights provide a new avenue for the tailoring and design of Fe-based FTO catalyst via adjustment of promoter contents.

■ ASSOCIATED CONTENT

Supporting Information

The Supporting Information is available free of charge on the ACS Publications website at DOI: 10.1021/acs.iecr.8b01795.

Tables S1–S2 and Figures S1 (PDF)

■ AUTHOR INFORMATION

Corresponding Author

*E-mail: xzduan@ecust.edu.cn. Phone: +86-21-64250937. Fax: +86-21-64253528.

ORCID

Xuezhi Duan: 0000-0002-5843-5950

Notes

The authors declare no competing financial interest.

■ ACKNOWLEDGMENTS

This work was supported by the Natural Science Foundation of China (21776077), Shanghai NSF (17ZR1407300 and 17ZR1407500), the Program for Professor of Special Appointment (Eastern Scholar) at Shanghai Institutions of Higher Learning, the Shanghai Rising-Star Program (17QA1401200),

and the 111 Project of the Ministry of Education of China (B08021). B.X.C. thanks support from China Scholarship Council (CSC) for his study at NTNU.

■ REFERENCES

- (1) Torres Galvis, H. M.; de Jong, K. P. Catalysts for production of lower olefins from synthesis gas: A review. *ACS Catal.* **2013**, *3*, 2130–2149.
- (2) Dry, M. E. The Fischer–Tropsch process: 1950–2000. *Catal. Today* **2002**, *71*, 227–241.
- (3) Schulz, H. Short history and present trends of Fischer–Tropsch synthesis. *Appl. Catal., A* **1999**, *186*, 3–12.
- (4) Janardanarao, M. Direct catalytic conversion of synthesis gas to lower olefins. *Ind. Eng. Chem. Res.* **1990**, *29*, 1735–1753.
- (5) Chen, W.; Lin, T. J.; Dai, Y. Y.; An, Y. L.; Yu, F.; Zhong, L. S.; Li, S. G.; Sun, Y. H. Recent advances in the investigation of nanoeffects of Fischer–Tropsch catalysts. *Catal. Today* **2018**, *311*, 8–22.
- (6) Cheng, K.; Kang, J. C.; King, D. L.; Subramanian, V.; Zhou, C.; Zhang, Q. H.; Wang, Y. Advances in catalysis for syngas conversion to hydrocarbons. *Adv. Catal.* **2017**, *60*, 125–208.
- (7) Zhang, Q. H.; Kang, J. C.; Wang, Y. Development of novel catalysts for Fischer–Tropsch synthesis: Tuning the product selectivity. *ChemCatChem* **2010**, *2*, 1030–1058.
- (8) Zhang, Q. H.; Deng, W. P.; Wang, Y. Recent advances in understanding the key catalyst factors for Fischer–Tropsch synthesis. *J. Energy Chem.* **2013**, *22*, 27–38.
- (9) Davis, B. H. Fischer–Tropsch synthesis: Comparison of performances of iron and cobalt catalysts. *Ind. Eng. Chem. Res.* **2007**, *46*, 8938–8945.
- (10) Ojeda, M.; Nabar, R.; Nilekar, A. U.; Ishikawa, A.; Mavrikakis, M.; Iglesia, E. CO activation pathways and the mechanism of Fischer–Tropsch synthesis. *J. Catal.* **2010**, *272*, 287–297.
- (11) Sun, B.; Xu, K.; Nguyen, L.; Qiao, M. H.; Tao, F. Preparation and catalysis of carbon-supported iron catalysts for Fischer–Tropsch synthesis. *ChemCatChem* **2012**, *4*, 1498–1511.
- (12) Wang, D.; Chen, B. X.; Duan, X. Z.; Chen, D.; Zhou, X. G. Iron-based Fischer–Tropsch synthesis of lower olefins: The nature of γ -Fe₃C₂ catalyst and why and how to introduce promoters. *J. Energy Chem.* **2016**, *25*, 911–916.
- (13) Torres Galvis, H. M.; Bitter, J. H.; Khare, C. B.; Ruitenbeek, M.; Dugulan, A. I.; de Jong, K. P. Supported iron nanoparticles as catalysts for sustainable production of lower olefins. *Science* **2012**, *335*, 835–838.
- (14) Torres Galvis, H. M.; Bitter, J. H.; Davidian, T.; Ruitenbeek, M.; Dugulan, A. I.; de Jong, K. P. Iron particle size effects for direct production of lower olefins from synthesis gas. *J. Am. Chem. Soc.* **2012**, *134*, 16207–16215.

- and sulfur on catalytic performance of supported iron catalysts for the Fischer–Tropsch synthesis of lower olefins. *J. Catal.* **2013**, *303*, 22–30.
- (16) Cheng, Y.; Lin, J.; Xu, K.; Wang, H.; Yao, X. Y.; Pei, Y.; Yan, S. R.; Qiao, M. H.; Zong, B. N. Fischer–Tropsch synthesis to lower olefins over potassium-promoted reduced graphene oxide supported iron catalysts. *ACS Catal.* **2016**, *6*, 389–399.
- (17) Zhou, X. P.; Ji, J.; Wang, D.; Duan, X. Z.; Qian, G.; Chen, D.; Zhou, X. G. Hierarchical structured α -Al₂O₃ supported S-promoted Fe catalysts for direct conversion of syngas to lower olefins. *Chem. Commun.* **2015**, *51*, 8853–8856.
- (18) Davis, B. H. Fischer–Tropsch synthesis: Relationship between iron catalyst composition and process variables. *Catal. Today* **2003**, *84*, 83–98.
- (19) de Smit, E.; Weckhuysen, B. M. The renaissance of iron-based Fischer–Tropsch synthesis: On the multifaceted catalyst deactivation behavior. *Chem. Soc. Rev.* **2008**, *37*, 2758–2781.
- (20) Zhai, P.; Xu, C.; Gao, R.; Liu, X.; Li, M. Z.; Li, W. Z.; Fu, X. P.; Jia, C. J.; Xie, J. L.; Zhao, M.; Wang, X. P.; Li, Y. W.; Zhang, Q. W.; Wen, X. D.; Ma, D. Highly tunable selectivity for syngas-derived alkenes over zinc and sodium-modulated Fe₂C₂ catalyst. *Angew. Chem., Int. Ed.* **2016**, *55*, 9902–9907.
- (21) Wang, C.; Wang, Q. X.; Sun, X. D.; Xu, L. Y. CO hydrogenation to light alkenes over Mn/Fe catalysts prepared by coprecipitation and sol-gel methods. *Catal. Lett.* **2005**, *105*, 93–101.
- (22) Ribeiro, M. C.; Jacobs, G.; Pendyala, R.; Davis, B. H.; Cronauer, D. C.; Kropf, A. J.; Marshall, C. L. Fischer–Tropsch synthesis: Influence of Mn on the carburization rates and activities of Fe-based catalysts by TPR-EXAFS/XANES and catalyst testing. *J. Phys. Chem. C* **2011**, *115*, 4783–4792.
- (23) Li, T. Z.; Wang, H. L.; Yang, Y.; Xiang, H. W.; Li, Y. W. Effect of manganese on the catalytic performance of an iron-manganese bimetallic catalyst for light olefin synthesis. *J. Energy Chem.* **2013**, *22*, 624–632.
- (24) Yang, Z. Q.; Pan, X. L.; Wang, J. H.; Bao, X. H. FeN particles confined inside CNT for light olefin synthesis from syngas: Effects of Mn and K additives. *Catal. Today* **2012**, *186*, 121–127.
- (25) Tian, Z. P.; Wang, C. G.; Si, Z.; Ma, L. L.; Chen, L. G.; Liu, Q. Y.; Zhang, Q.; Huang, H. Y. Fischer–Tropsch synthesis to light olefins over iron-based catalysts supported on KMnO₄ modified activated carbon by a facile method. *Appl. Catal., A* **2017**, *541*, 50–59.
- (26) Yuan, Y.; Huang, S. Y.; Wang, H. Y.; Wang, Y. F.; Wang, J.; Lv, J.; Li, Z. H.; Ma, X. B. Monodisperse nano-Fe₃O₄ on α -Al₂O₃ catalysts for Fischer–Tropsch synthesis to lower olefins: Promoter and size effects. *ChemCatChem* **2017**, *9*, 3144–3152.
- (27) Ngantsoue-Hoc, W.; Zhang, Y. Q.; O'Brien, R. J.; Luo, M. S.; Davis, B. H. Fischer–Tropsch synthesis: Activity and selectivity for Group I alkali promoted iron-based catalysts. *Appl. Catal., A* **2002**, *236*, 77–89.
- (28) Luo, M. S.; O'Brien, R. J.; Bao, S. Q.; Davis, B. H. Fischer–Tropsch synthesis: Induction and steady-state activity of high-alpha potassium promoted iron catalysts. *Appl. Catal., A* **2003**, *239*, 111–120.
- (29) Duan, X. Z.; Wang, D.; Qian, G.; Walmsley, J. C.; Holmen, A.; Chen, D.; Zhou, X. G. Fabrication of K-promoted iron/carbon nanotubes composite catalysts for the Fischer–Tropsch synthesis of lower olefins. *J. Energy Chem.* **2016**, *25*, 311–317.
- (30) Wang, D.; Zhou, X. P.; Ji, J.; Duan, X. Z.; Qian, G.; Zhou, X. G.; Chen, D.; Yuan, W. K. Modified carbon nanotubes by KMnO₄ supported iron Fischer–Tropsch catalyst for the direct conversion of syngas to lower olefins. *J. Mater. Chem. A* **2015**, *3*, 4560–4567.
- (31) Wang, D.; Ji, J.; Chen, B. X.; Chen, W. Y.; Qian, G.; Duan, X. Z.; Zhou, X. G.; Holmen, A.; Chen, D.; Walmsley, J. C. Novel Fe/MnK-CNTs nanocomposites as catalysts for direct production of lower olefins from syngas. *AIChE J.* **2017**, *63*, 154–161.
- (32) Zhang, C. H.; Yang, Y.; Teng, B. T.; Li, T. Z.; Zheng, H. Y.; Xiang, H. W.; Li, Y. W. Study of an iron-manganese Fischer–Tropsch synthesis catalyst promoted with copper. *J. Catal.* **2006**, *237*, 405–415.
- (33) Oschatz, M.; Krans, N.; Xie, J. X.; de Jong, K. P. Systematic variation of the sodium/sulfur promoter content on carbon-supported iron catalysts for the Fischer–Tropsch to olefins reaction. *J. Energy Chem.* **2016**, *25*, 985–993.
- (34) Fu, D. L.; Dai, W. W.; Xu, X. C.; Mao, W.; Su, J. J.; Zhang, Z. P.; Shi, B. F.; Smith, J.; Li, P.; Xu, J.; Han, Y. F. Probing The Structure Evolution of Iron-Based Fischer–Tropsch to Produce Olefins by Operando Raman Spectroscopy. *ChemCatChem* **2015**, *7*, 752–756.
- (35) Lou, F. L.; Zhou, H. T.; Huang, F.; Vullum-Bruer, F.; Tran, T. D.; Chen, D. Facile synthesis of manganese oxide/aligned carbon nanotubes over aluminium foil as 3D binder free cathodes for lithium ion batteries. *J. Mater. Chem. A* **2013**, *1*, 3757–3767.
- (36) Ma, S. B.; Ahn, K. Y.; Lee, E. S.; Oh, K. H.; Kim, K. B. Synthesis and characterization of manganese dioxide spontaneously coated on carbon nanotubes. *Carbon* **2007**, *45*, 375–382.
- (37) Barkhuizen, D.; Mabaso, I.; Viljoen, E.; Welker, C.; Claeys, M.; van Steen, E.; Fletcher, J. C. Q. Experimental approaches to the preparation of supported metal nanoparticles. *Pure Appl. Chem.* **2006**, *78*, 1759–1769.
- (38) Das, D.; Ravichandran, G.; Chakrabarty, D. K. Conversion of syngas to light olefins over silicalite-1 supported iron and cobalt catalysts: Effect of manganese addition. *Catal. Today* **1997**, *36*, 285–293.
- (39) Malek Abbaslou, R. M.; Tavasoli, A.; Dalai, A. K. Effect of pre-treatment on physico-chemical properties and stability of carbon nanotubes supported iron Fischer–Tropsch catalysts. *Appl. Catal., A* **2009**, *355*, 33–41.
- (40) Chen, W. Y.; Ji, J.; Duan, X. Z.; Qian, G.; Li, P.; Zhou, X. G.; Chen, D.; Yuan, W. K. Unique reactivity in Pt/CNT catalyzed hydrolytic dehydrogenation of ammonia borane. *Chem. Commun.* **2014**, *50*, 2142–2144.
- (41) Sadezky, A.; Muckenhuber, H.; Grothe, H.; Niessner, R.; Poschl, U. Raman microspectroscopy of soot and related carbonaceous materials: Spectral analysis and structural information. *Carbon* **2005**, *43*, 1731–1742.
- (42) Koeken, A. C. J.; Torres Galvis, H. M.; Davidian, T.; Ruitenbeek, M.; de Jong, K. P. Suppression of carbon deposition in the iron-catalyzed production of lower olefins from synthesis gas. *Angew. Chem., Int. Ed.* **2012**, *51*, 7190–7193.
- (43) Xie, J. X.; Yang, J.; Dugulan, A. I.; Holmen, A.; Chen, D.; de Jong, K. P.; Louwse, M. J. Size and promoter effects in supported iron Fischer–Tropsch catalysts: Insights from experiment and theory. *ACS Catal.* **2016**, *6*, 3147–3157.
- (44) Gueudré, L.; Thegarid, N.; Burel, L.; Jouguet, B.; Meunier, F.; Schuurman, Y.; Mirodatos, C. Coke chemistry under vacuum gasoil/bio-oil FCC co-processing conditions. *Catal. Today* **2015**, *257*, 200–212.
- (45) Collett, C. H.; McGregor, J. Things go better with coke: The beneficial role of carbonaceous deposits in heterogeneous catalysis. *Catal. Sci. Technol.* **2016**, *6*, 363–378.